ACS APPLIED NANO MATERIALS

www.acsanm.org Article

Plasma-Assisted N-Doped TiO_2 Nanotube Array as an Active UV−vis Photoanode

Marcin Pisarek,* Mirosław Krawczyk, Magdalena Gurgul, Leszek Zaraska, Krzysztof Bieńkowski, Marcin Hołdyński, and Renata Solarska

Cite This: *ACS Appl. Nano Mater.* 2023, 6, 10351−10364 Read Online

ACCESS | Metrics & More | Article Recommendations | Supporting Information

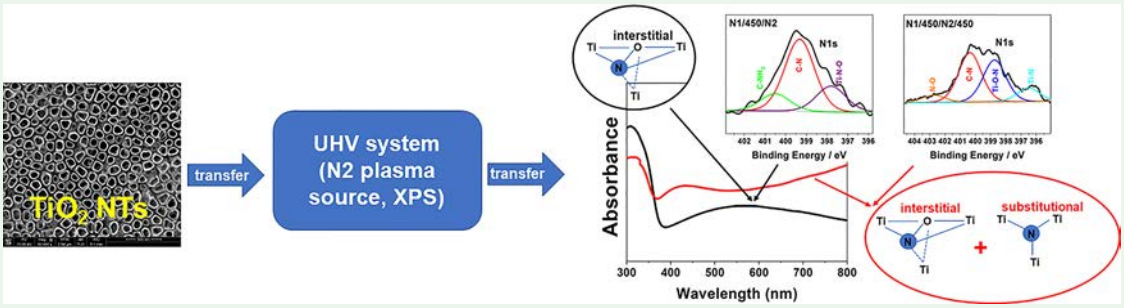

ABSTRACT: This work shows the possibility of using plasma nitriding under ultra-high-vacuum conditions to introduce nitrogen into a titanium dioxide structure in the form of nanotubes with a diameter of about 110 nm. Nanotubes were produced by the anodic oxidation of Ti foil in a solution based on glycerine and water with the addition of ammonium fluoride at a voltage of 25 V. Based on experimental evidence obtained by X-ray photoelectron spectroscopy (XPS, in situ), it has been shown that alternating nitriding and annealing processes at 450 °C leads to formation of Ti-N-O, Ti-N, and Ti-O-N chemical bonds in the TiO_2 crystal structure (anatase). The observed changes were identified as interstitial or substitutional admixtures or variations of these. The spectrophotometric and spectrophotoelectrochemical tests performed showed that the photoactivity of the photoanodes doped with nitrogen and annealed at 450 °C in the UV−vis range was significantly greater than that of the photoanodes without nitrogen. The highest maximum photocurrent density, of about 30.0 $\mu A \cdot cm^{-2}$ at a wavelength of λ = 350 nm, was obtained for the double-nitrided and once-annealed sample, where nitrogen was mainly incorporated in the interstitial positions in the TiO_2 lattice. For the materials not nitrided as well as annealed only at 450 °C and pristine, the worse photoresponse was received at the levels of ∼16 and ∼0.2 $\mu A \cdot cm^{-2}$, respectively. The thermo-chemical treatment applied also effectively extended the operational range of the photoanodes toward visible light, where a wide maximum of light absorption was observed from ∼400 to ∼700 nm, with a maximum wavelength of 550 nm and an estimated bandgap energy of 2.5 eV. Our investigations confirmed that photoelectrochemical (PEC) performance for TiO_2 NT-based photoanodes was achieved by the optimum annealing condition and concentration of nitrogen, where the narrowed bandgap was observed by generating a new N 2p energy level above the O 2p valence band. The following research techniques were used to identify the changes taking place in the materials produced: XPS spectroscopy, UV−vis spectroscopy, PEC measurements, X-ray diffraction structural measurements, and scanning electron microscopic observations.

KEYWORDS: *nanotubes, titanium dioxide, plasma nitriding, in situ XPS analysis, photoanodes, UV−vis analysis, photoelectrochemical investigations*

INTRODUCTION

Doping semiconductor materials with non-metallic ions such as C, N, or S is a typical way of modifying their electronic structure,[1−7] which ultimately leads to a reduction in the bandgap energy (E_g). The width of the energy gap and its position relative to the Fermi level are of fundamental importance to the properties of semiconductors. For several decades, titanium dioxide has been considered as one of the most promising photocatalysts; Fujishima and Honda first performed photoelectrochemical (PEC) water splitting using this material in 1972.[8] As a result of photon absorption, an electron migrates from the valence band to the conduction band, leaving a hole in the valence band, which results in the formation of charge carriers (electron−hole pairs). These can recombine in the crystal lattice (directly or indirectly) or

Received: March 22, 2023
Accepted: May 30, 2023
Published: June 13, 2023

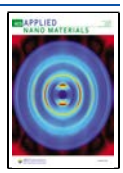

migrate to the surface of the photocatalyst where they participate in redox reactions with adsorbed organic compounds and adsorbed oxygen.[3,5,9,10] However, it is known that the practical use of TiO_2 in such processes is limited due to the wide bandgap (E_g = 3.0−3.2 eV).[3,5,9,11−13] Moreover, the generation of electrons in the conduction band and of holes in the valence band under the influence of visible light is inefficient. With such a wide bandgap, TiO_2 can only be excited by photons of wavelengths shorter than 390 nm appearing in the ultraviolet (UV) region.[14,15] In fact, this range covers only a few percent of the visible light spectrum.[3,14] A most common research method that can effectively increase the absorption range of visible light is doping with nitrogen.[5,14] This is due to the fact that nitrogen atoms can be effectively introduced into the TiO_2 lattice, creating a new N 2p energy level above the O 2p valence band (known as the impurity band), thereby changing the width of the energy gap. Ultimately, this leads to a shift in optical response toward the visible range.[1,3,14,16] This is possible because the replacement of oxygen atoms in the TiO_2 lattice with nitrogen atoms is effective due to their similar size and relatively low ionization energy and to the stability of the Ti−N−O bonds that are formed.[13,14,16,17] It is well known that photocatalytic processes involving TiO_2 are heterogeneous and that the surface area of the catalyst plays an important role. The structural properties of TiO_2, such as its crystallinity, particle size, grain size, porosity, and surface area, are all affected by the TiO_2 synthesis method, doping method, and the type of dopant.[2,3,18−21] Therefore, nanostructures based on TiO_2 nanotubes obtained by the anodic oxidation of titanium have been widely used in recent years as photocatalysts (photoanodes) due to their particular properties.[21] Such materials are characterized by strong light-scattering effects due to their characteristic morphology, that is, densely packed tubes of a certain height that can be separated from each other.[2,20−24] In addition, highly ordered nanotubes that are vertically oriented to the metallic Ti substrate[25] provide a high degree of electron mobility along the axis of the tubes—a unidirectional charge transfer.[18,26,27] Another advantage is that it is relatively easy to control their crystalline form or degree of crystallinity (anatase, rutile, and a mixture of anatase and rutile) through temperature processes.[20,25,28−30] These properties have been used effectively in various types of light-induced reactions, such as degradation of various types of dyes (methylene orange,[31,32] methylene blue,[33−36] rhodamine B,[13] and azo dye (RB5)[37]), pesticides (acephate[11]), phenols,[27] and the production of hydrogen.[10,13,31,38−41] Despite these advantages, a limitation in the use of nanotubes in photocatalysis as broadly understood is the nature of titanium oxide itself, and therefore its physical and chemical properties, as mentioned above. In addition, TiO_2-based photocatalysts are characterized by a relatively fast recombination of electron−hole pairs on the surface, which limits the efficiency of photoconversion processes.[3] The nitrogen atoms introduced into the TiO_2 structure may reduce the recombination of charges by stabilizing the electron−hole pairs generated and at the same time maintain the original structure of TiO_2.[13,17,42,43] Taking the above into account, an attempt was made to effectively introduce nitrogen into the structure of TiO_2 nanotubes by plasma nitriding under ultra-high-vacuum (UHV) conditions in order to reduce the amount of chemisorbed N_2 molecules on the surface of the tested materials. This type of selective nitrogen doping leads to a significant improvement in TiO_2 photoconversion processes over a wide UV−vis range by generating new N 2p states or a mixture of N 2p and O 2p orbital electron states, i.e., discrete energy levels at the upper edge of the valence band.[1,42−46] This is possible when nitrogen is called a substitutional or interstitial dopant in the TiO_2 lattice, which has been confirmed by density functional theory (DFT) calculations or in accordance with the first rules (ab initio)[45,47] related to determining their electronic structure.[1,15,45,47,48] The calculations showed that both types of doping are possible and lead to a narrowing of the bandgap. Despite the theoretical calculations that have been made[45,47] and much experimental data, including X-ray photoelectron spectroscopy (XPS),[1,6,11,49−51] the nitrogen-doping mode in the TiO_2 lattice is still unclear and contains many complex problems resulting from the method of introducing nitrogen into the TiO_2 network (chemical and physical methods).[1,3,21] Therefore, the aim of this work included the investigation of PEC properties depending on the nitrogen-doping procedure and the impact of that mechanism on the photocurrent response of the resulting materials. In such cases, the modified surface of TiO_2 NT-based photocatalysts plays a key role. Consequently, controlling the doping process is essential since it can yield different results in terms of photocatalytic performance. The proposed optimization of the plasma-nitriding process in UHV conditions creates such opportunities. Figure 1 shows in a schematic way the process of producing photoanodes used for photocatalytic tests.

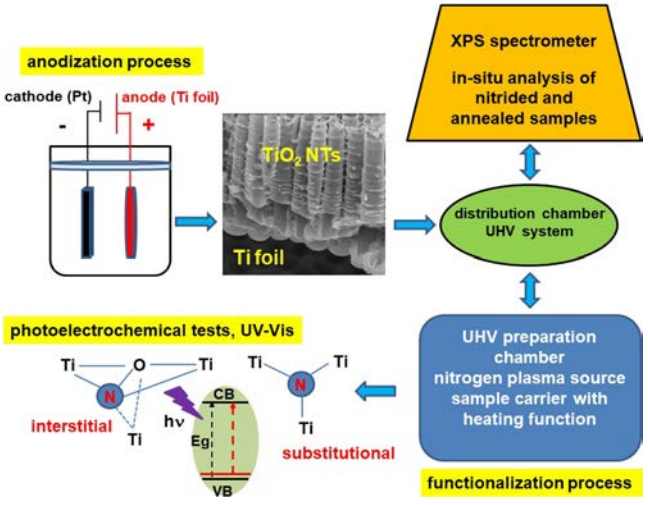

Figure 1. Scheme showing the methodology of photoanode production along with the research methods used.

EXPERIMENTAL SECTION

Sample Preparation. *TiO_2 NT Formation.* TiO_2 nanotubes (NTs) were fabricated in a one-step anodization process on Ti foil (0.25 mm-thick and 99.5% + % purity, Alfa Aesar) at 25 V for 3 h in an optimized electrolyte based on the glycerol and water mixture (volume ratio 50:50) containing 0.27 M ammonium fluoride (NH_4F) by using a two-electrode electrochemical system (anode—titanium foil with an area of about 1 cm^2, cathode—a platinum mesh with an area of about 1 cm^2). After the anodization process, all the samples were rinsed with DI water (soaking for 24 h) and dried in air.[24]

Nitriding Proces. Plasma nitriding is conducted in a UHV preparation chamber (PREVAC, Rogów, Poland) at 1.3×10^{-5} mbar pressure of flowing nitrogen and at low temperatures (less than 40 °C). Nitrogen plasma is produced using a PCS-ECR plasma cracker

https://doi.org/10.1021/acsanm.3c01278
ACS Appl. Nano Mater. 2023, 6, 10351−10364

source (SPECS Surface Nano Analysis GmbH, Berlin, Germany), which is a compact electron cyclotron resonance (ECR) ion source. Microwaves at a frequency of 2.45 GHz and a power of 60 W are generated. After a 4 h nitriding treatment, some of the samples were annealed in vacuum conditions (10^{-8} mbar vacuum pressure) at 450 °C for 2 h. The samples were then transferred in situ to an XPS analysis chamber for surface chemical analysis.[24] The samples were investigated in the following order after the individual stages of functionalization:

The assigned designations to the TiO_2 NTs samples were used in the description of the research results in order to simplify the nomenclature (Table 1).

Table 1. Markings of the Investigated Samples

samples (photoanodes)	nomenclature
TiO_2 NTs	pristine
TiO_2 NTs + N_2	N1
TiO_2 NTs + N_2 + 450 °C	N1/450
TiO_2 NTs + N_2 + 450 °C + N_2	N1/450/N2
TiO_2 NTs + N_2 + 450 °C + N_2 + 450 °C	N1/450/N2/450
TiO_2 NTs + 450 °C (reference sample)	450

Sample Characterization. *X-ray Photoelectron Spectroscopy.* The chemical states of individual elements were verified using XPS on a PHI 5000 VersaProbe (ULVAC-PHI) spectrometer. For this purpose, monochromatic AlKα ($h\nu$ = 1486.6 eV, power 25 W, voltage 15 kV) radiation was used as the X-ray excitation source at a lateral resolution of about 100 × 100 μm. High-resolution XPS spectra for individual elements were recorded using the following parameters: pass energy 23.5 eV and energy step size 0.1 eV. Avantage-based data system software (Version 5.9911, Thermo Fisher Scientific, Waltham, MA, USA) was used to process the data, where a Smart function of background subtraction was used to obtain the XPS signal intensity. All the XPS peaks collected were fitted using an asymmetric Gaussian/Lorentzian mixed function at a constant G/L ratio of 0.35 (±0.05). The binding energies (BEs) measured were corrected with reference to the energy of the C 1s peak at 285.0 eV.[24]

Scanning Electron Microscopy. An FEI Nova NanoSEM 450 SEM microscope was used to characterize the morphology of the received samples. Scanning electron microscopy (SEM) was carried out using the Through Lens Detector (TLD) of secondary electrons at a primary beam energy of 5 or 10 kV under high vacuum (pressure 10^{-6} mbar). After the inspection region had been chosen, SEM images were obtained at a long-scan acquisition time of typically 30 s per frame.[24]

X-ray Diffraction. X-ray powder diffraction data were collected on a PANalytical Empyrean diffractometer fitted with a X'Celerator detector using Ni-filtered Cu Kα radiation (λ_1 = 1.54056 Å and λ_2 = 1.54439 Å). Data were collected on a flat plate θ/θ geometry on a spinning sample holder. All the data presented were collected in the 2θ range 10–90°, at an interval of 0.0167°, with a scan time of 30 s per interval.

UV–vis Spectroscopy. Optical absorption spectra of the functionalized TiO_2 NTs were acquired using a Jasco V-650 spectrophotometer equipped with a 16 mm integrating sphere using diffuse reflectance spectroscopy methodology. The bandgaps were calculated using the Kubelka–Munk equation.

Photoelectrochemical Measurements. To evaluate the influence of nitrogen doping on the photoelectrochemical properties of TiO_2, materials were subjected to tests in a Teflon cell with a quartz window using a photoelectric spectrometer equipped with a 150 W xenon arc lamp combined with a potentiostat (Instytut Fotonowy). All the measurements were performed in a 0.1 M KNO_3 solution, in a three-electrode system, where a saturated calomel electrode, a platinum wire, and the TiO_2–N_2 samples were used as the reference, counter, and working electrodes, respectively. Photoelectrochemical measurements were carried out using a pulsed exposure to illumination with monochromatic light (in a range of 300–600 nm) with a step of 10 nm. During all the tests, a potential in a range of 0–1 V vs SCE (with a step of 0.2 V) was applied. The photocurrent values were converted to incident photon to current efficiency (IPCE) using the following equation:

$$\mathrm{IPCE} = 1240\frac{J_p(\lambda)}{\lambda\, P(\lambda)} \quad (1)$$

where J_p (λ) is the photocurrent density recorded at a particular wavelength (λ) and P (λ) is the power density of the incident light at a particular wavelength (λ).

The stability of photoanodes was evaluated by measuring the photocurrents during 30 min of illumination with a Xe lamp using the same experimental setup.

RESULTS AND DISCUSSION

Figure 2a shows a typical morphology (top view) of titanium oxide nanotubes immediately after anodic oxidation at 25 V in a solution of glycerine, water, and ammonium fluoride.

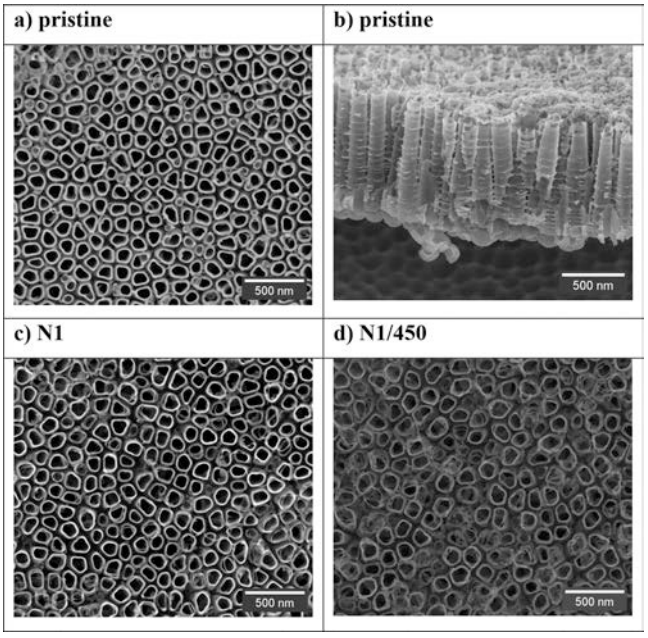

Figure 2. SEM images of TiO_2 NTs after anodic oxidation (a—top view, b—cross-sectional view), after plasma nitriding in UHV conditions (c), and after annealing at 450 °C (d).

The SEM images reveal that the tubes are densely packed and form a honeycomb-like structure. The tubes are about 110 nm tall, with a wall thickness of about 20 nm, and their growth takes place perpendicularly to the Ti substrate, as shown in our previous work,[23] Figure 2a,b. Further functionalization of the nanotubes in situ as a result of plasma nitriding and heating at 450 °C in the UHV preparation chamber did not significantly affect their morphology,[21,24] Figure 2c, d. Nevertheless, thermal treatment does lead in particular to other significant changes related to the transformation of TiO_2 nanotubes from an amorphous form into a crystalline form—anatase, as shown in Figure 3. Clearly visible peaks of the Ti substrate are associated with the direct growth of nanotubes on titanium foil, see Figure 2b. The sample subjected to heat treatment at 450 °C in UHV conditions shows extra three distinct peaks at about 2θ = 25.0°, 48.0°, and 55.0° corresponding to anatase reflections (101), (200), and (211), respectively.[20]

https://doi.org/10.1021/acsanm.3c01278
ACS Appl. Nano Mater. 2023, 6, 10351–10364

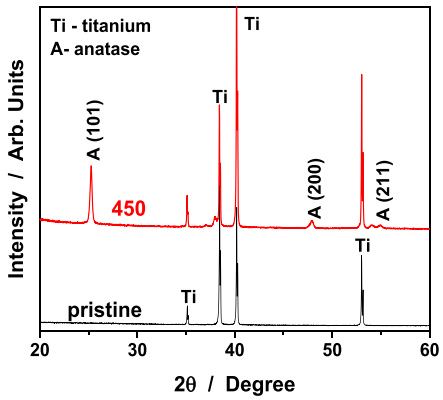

Figure 3. XRD patterns for TiO_2 NTs in the as-received state and after heat treatment in UHV conditions at 450 °C/2 h.

Data in the literature show that such a transformation can occur in this type of material at a temperature above 280 °C,[30] and at 450 °C, a fully crystallized anatase phase is obtained.[25,28,52] This is one of the important properties of titanium dioxide, whose polymorphism is used in a practical way in photocatalytic applications, because fully crystalline titanium dioxide (anatase, a mixture of anatase and rutile, and rutile) can only be used in practice.[1,3,9] Even though rutile is the most stable crystallographic form of TiO_2, in UV−vis light-induced studies, the anatase structure or a mixture of anatase and rutile is commonly used.[9,14] This is because the degree of recombination of the electron−hole pair system is much lower in anatase than in rutile,[2,3,9,13] and the phase mixture can improve photocatalytic performance due to increased charge separation and can inhibit recombination.[2,3,9,13] In addition, anatase has the smallest refractive index (~2.5) of the three TiO_2 polymorphs, a higher edge of optical absorption than rutile, and the largest specific surface area (from 50 to 120 m^2/g).[53] Nevertheless, it is characterized by the largest bandgap—about 3.2 eV—even though for all titanium dioxide species, the location of the valence band is the same (anatase, rutile, brookite),[9] and the main differences result from the location of the conduction band. As already mentioned, the minimum energy needed for anatase to excite an electron and generate a hole in the valence band (E_g) is about 3.2 eV, which corresponds to a quantum of radiation with a wavelength of ~390 nm.[14] TiO_2, therefore, can be activated only in the UV range.[1−3,9] The range of radiation needed to excite the photocatalyst poses a serious limitation on the large-scale application of TiO_2. The introduction of a nitrogen dopant into the crystallographic structure of TiO_2 can change this.[21]

Nitrogen was introduced into the lattice of the TiO_2 nanotubes by means of a multi-stage controlled process of plasma nitriding combined with annealing at 450 °C. Figure 4 shows high-resolution XPS spectra for Ti 2p, O 1s, N 1s, and VB recorded after successive stages of nitrogen doping in situ. Before the nitriding process, the chemical composition of the surfaces of the nanotubes in the initial state (pristine) was determined. Data analysis of the spectra for Ti 2p, O 1s, N 1s, and VB (Figure 4a−d) showed that the basic chemical compound of the nanotubes was titanium dioxide, as proved by the characteristic spectral lines for Ti 2p (Ti $2p_{3/2}$ 458.8 eV, Ti $2p_{1/2}$ 464.5 eV) and O 1s (530.2 eV).[24,33,51] Moreover, taking into account the ratio of O 1s (530.2 eV)/Ti $2p_{3/2}$ (458.8 eV), which is 1.92, it seems that an almost fully stoichiometric TiO_2 was obtained. This was also confirmed by the shape of the XPS-VB spectrum with two broad bands that are O 2p in character, with the position of the edge of the valence band at around 3.0 eV.[24,54] The presence of typical carbon, oxygen, and nitrogen bonds was also found on the surface of the tubes (C−C: 284.5 eV; C−H: 285.0 eV; C−O/C−N: 286.0 eV; C═O: 287.1 eV; O═C−OH: 289, 0 eV; C−N: 399.9 eV; C−NH_3: 401.5 eV), which can be attributed to contaminations from the sample preparation. This is shown by the locations of the additional oxygen signals above the BE of 531.0 eV.[24,27,30] For the sample in the initial state, a fluorine peak (F 1s) was also recorded.[30] Its origin is related to the presence of ammonium fluorides in the electrolyte used to form the nanotubes by anodic oxidation of the Ti foil. The pristine material was further modified as a result of the plasma nitriding, as shown in Figure 4e−h (N1).

As in the case of the sample in the initial state after nitriding, the position of the maximum peaks for Ti 2p (Ti $2p_{3/2}$ 458.8 eV, Ti $2p_{1/2}$ 464.5 eV) and O 1s (530.2 eV) after deconvolution did not change. This corresponds to the BE values for TiO_2. However, there was an additional N 1s nitrogen peak at around 400 eV. A detailed analysis of this peak showed three states of nitrogen at the BE: 400.1, 399.0, and 401.1 eV. These states refer to chemisorbed nitrogen compounds (C−N) on the surface of the nanotubes,[21,22,24,33] nitrogen located in the TiO_2 network in the form of Ti−O−N bonds,[13,15,17,24] and nitrogen in the form of adsorbed C−NH_3,[15,33,43] respectively. The absence of typical Ti−N bonds is related to the fact that nanotubes have an amorphous structure immediately after anodic oxidation[30] (see Figure 3), so the formation of Ti−N bonds may be accidental. Such a structure is characterized by a rather chaotic arrangement of Ti and O atoms (no long-range order), although it may contain a small proportion of crystal phase domains. Therefore, it is most likely that the nitriding process in this case could have led to the formation of various types of bonds between oxygen, titanium, and nitrogen, forming compounds of unknown stoichiometry (e.g., TiO_xN_y) and, possibly, NO_x admixtures. The shape of the XPS-VB spectrum did not change significantly after nitriding, which means there were no structural or electronic changes in the tested material. Nevertheless, the advantage of an amorphous structure is that it is easier to introduce all kinds of nitrogen impurities.[24] This made it possible to introduce nitrogen into TiO_2 at a level of about 4.2 at %. To correct this effect, the sample of N1 was annealed in situ at 450 °C for 2 h under UHV conditions. Figure 4i−l shows XPS spectra for the Ti 2p, O 1s, N 1s, and VB after heat treatment (N1/450). The spectra recorded for individual elements have certain features that distinguish them from the spectra after nitriding. For both the Ti 2p and O 1s peaks, one can clearly see a shift of their main maxima toward larger BEs of about 0.5 eV compared with the previous samples, which is related to the change in the structure of the nanotubes from an amorphous to the crystalline form—anatase (see Figure 3). This shift may also be associated with a slight change in the lattice parameter of anatase itself as a result of nitrogen being introduced directly into the crystallographic structure of TiO_2 as a interstitial impurity, as has been suggested by other researchers.[15,27,43,55] In our case, no such effect was observed, as shown in our XRD structural studies for the nitrided and annealed samples (Figure S1 in the Supporting Information). However, the doping effect can be clearly seen in the N 1s nitrogen spectrum, where an evident change in the shape of the spectrum, and a change in the

https://doi.org/10.1021/acsanm.3c01278
ACS Appl. Nano Mater. 2023, 6, 10351−10364

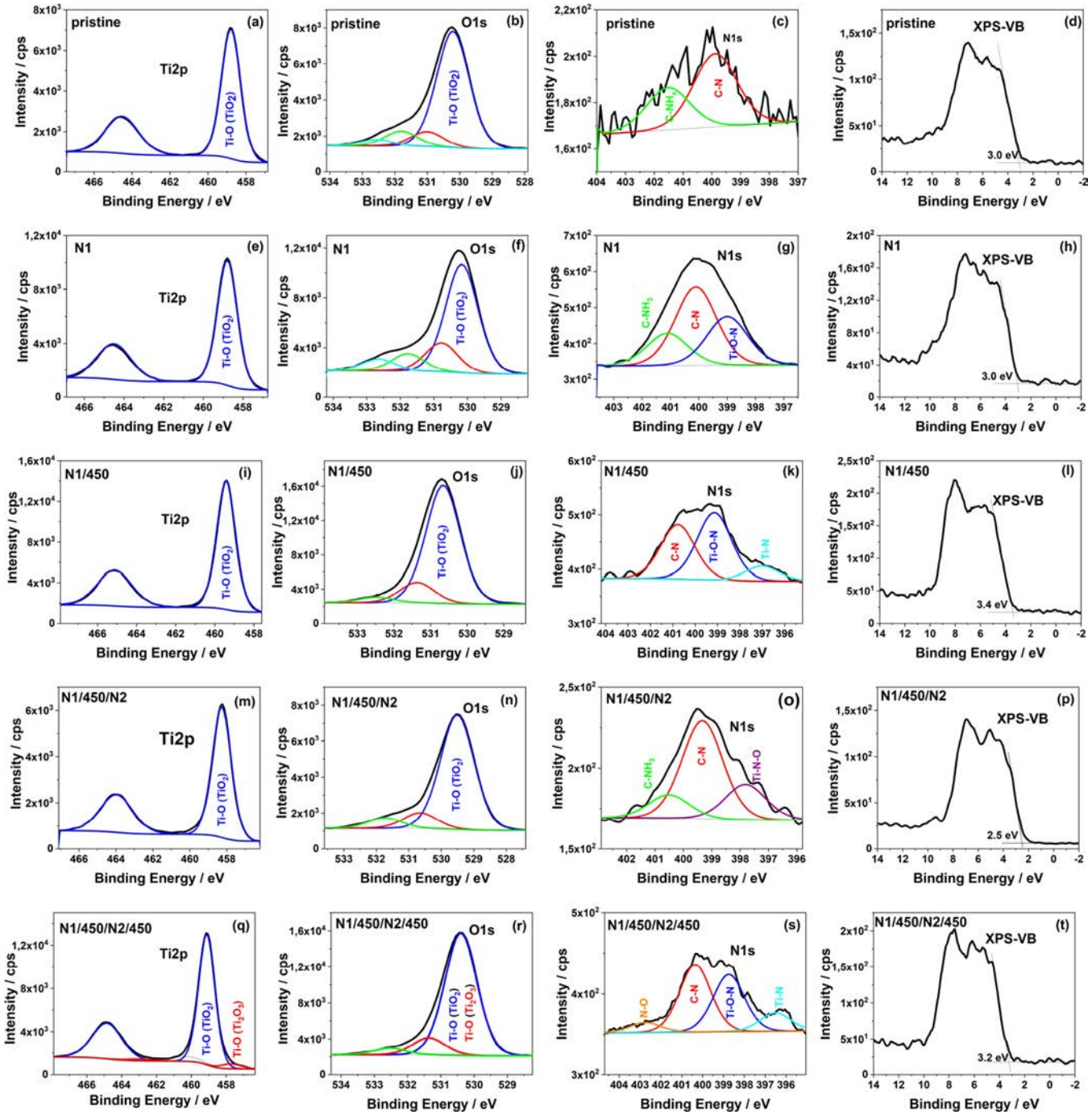

Figure 4. XPS spectra of Ti 2p, O 1s, N 1s, and XPS-VB recorded after various stages of titanium dioxide nanotube functionalization: pristine material (a–d), first plasma nitriding in UHV conditions—N1 (e–h), annealing at 450 °C in UHV conditions—N1/450 (i–l), second plasma nitriding in UHV conditions—N1/450/N2 (m–p), annealing at 450 °C in UHV conditions—N1/450/N2/450 (q–t). All of the XPS spectra were recorded in situ.

positions of individual signal maxima after deconvolution, can be observed. These individual peaks can be attributed to the presence of Ti–N bonds (397.0 eV—substitution nitrogen), Ti–O–N (399.1 eV—interstitial nitrogen), and chemisorbed nitrogen on the nanotube surface (400.8 eV).[15,21,22,33,43,46,51] Comparing the XPS spectra of nitrogen N 1s after single nitriding and annealing, certain changes can be seen, namely, the content of nitrogen effectively introduced into the anatase network as a permanent impurity is higher (60%) than in the case of the amorphous structure (30%), with a contribution of about 10% Ti–N bonds. The quantitative data also showed that, after annealing, a general decrease in nitrogen concentration was observed, to a level of about 2.2 atomic %, which is related to the removal of part of the nitrogen chemisorbed to the surface of the nanotubes during the annealing process.[36] Haryński et al. obtained similar results for plasma-nitrided samples, where the nitrogen plasma-induced crystallization of the anodic TiO_2 nanotube method was used, without thermal treatment.[21] The change in the structure of the nanotubes as a result of thermal treatment is also evidenced

https://doi.org/10.1021/acsanm.3c01278
ACS Appl. Nano Mater. 2023, 6, 10351–10364

by the change in the shape of the XPS-VB spectrum. The nature of this spectrum, which is dominated by two broad peaks of the O 2p-Ti 3d-hybridized states related to the nonbonding (~5 eV) and bonding (~8 eV) O 2p orbitals, respectively, is correlated with the crystallographic structure of anatase.[24,56−60] In addition, the estimated bandgap, based on the linear extrapolation of the edge of the lowest emission energy of the valence band,[24,56] is about 3.4 eV, which is close to the theoretical value for anatase (E_g = 3.2 eV). Further functionalization was aimed at re-introducing nitrogen into the structure of TiO_2 nanotubes by plasma nitriding (N2) but with a strictly defined crystallinity (N1/450). In Figure 4m−p, the spectra for Ti 2p, O 1s, N 1s, and VB are shown again. Interestingly, after the second stage of nitriding (N1/450/N2), the maxima of the Ti 2p and O 1s peaks changed their position toward lower BE values. The BEs as determined for Ti 2p were 458.3 eV (Ti $2p_{3/2}$) and 464.0 eV (Ti $2p_{1/2}$) and for O 1s 529.5 eV. The maxima of these peaks indicate the presence of Ti^{4+} and O^{2-} in the structure of TiO_2.[15,27,33,42] Yet, another change was observed in the nitrogen peak, for which the main peak was found at 399.3 eV, which can be attributed to chemisorbed nitrogen on the surface of the nanotubes, in accordance with our previous observations. Nevertheless, some literature data also indicate that, for this BE, the presence of interstitial nitrogen (Ti−O−N) has been identified.[3,13,15,43,50] In addition, for this sample, a signal at the BE of 400.5 eV may suggest the presence of adsorbed nitrogen in the form of C−NH_3 as for the sample in the initial state (pristine).[15,33,43] The unambiguous change in the interstitial nitrogen doping of the TiO_2 lattice can be attributed to the peak maximum at an energy of 397.8 eV. This is probably an intermediate state between nitride (397.0 eV) and oxynitride (399.0 eV), which can be defined as Ti−N−O (TiN_xO_y).[51] The appearance of such bonds causes a decrease in the electron density of nitrogen in TiN due to the high electronegativity of oxygen, which may also generate a shift in the maximum of the Ti 2p and O 1s peaks toward lower BE values.[3,13,15] This behavior is related to the mechanism of nitrogen doping of the TiO_2 structure, where a N atom bonds with three Ti atoms by replacing the O atom in the TiO_2 lattice or N atoms occupy interstitial sites where a N atom is bonded to one or more O atoms.[45] The second stage of nitriding clearly affected the electronic structure of TiO_2 as the edge of the valence band shifted toward a lower BE as determined from the XPS-VB spectrum to about 2.5 eV. This change may be related to the fact that interstitial doping leads to the addition of nitrogen in the TiO_2 crystal lattice, in contrast to substitutional doping.[44,45] Therefore, a larger amount of nitrogen can be effectively introduced into the TiO_2 structure, which can lead to a reduced energy gap. The XPS experimental data obtained after the two-stage plasma nitriding process are very similar to the observations of other researchers who also used a two-stage modification of titanium oxide with nitrogen, where the primary source of N was nitric acid and the secondary source urea.[43] Boningari et al. observed that the dominant signal of nitrogen N 1s was a peak at a BE of about 399.2 eV, regardless of the chosen procedure or the amount of nitrogen introduced into the TiO_2 lattice. They attributed this peak to the position of interstitial nitrogen in the oxide structure (Ti−O−N).[43] Analyzing the spectra of N 1s after plasma nitriding, a similar effect (trend) can be observed. The only difference is in a slightly different peak position assigned with interstitial nitrogen, which in our case varied from 397.8 to 399.1 eV. This difference is due to the different method used to introduce nitrogen into the TiO_2 lattice. The last stage of functionalization was re-annealing the sample at 450 °C (Figure 4q−t; N1/450/N2/450). a Secondary thermal treatment at 450 °C causes a change in the position of the peak maxima for Ti2p and O1s again, this time towards higher values of the BEs (Ti $2p_{3/2}$ 459.1 eV, Ti $2p_{1/2}$ 464.8 eV, and O 1s 530.4 eV). Nevertheless, secondary annealing led to the appearance of an additional signal in the Ti 2p spectrum, which can be attributed to Ti^{3+} (Ti $2p_{3/2}$ 457.7 eV, Ti $2p_{1/2}$ 463.0 eV).[27,51] The appearance of this signal was the result of the double annealing process of the nanotubes at a temperature of 450 °C in vacuum conditions. These nonstoichiometric oxides can modify the electronic structure of TiO_2 by creating a donor level below the conduction band (oxygen vacancies), which in turn can affect the rate of recombination of electron−hole pairs and effectively extend the range of visible light absorption.[3,15,61] It is also worth noting that, after the secondary annealing, the spectrum of nitrogen, in a bond energy range of 404.5−395.5 eV, was similar in shape to the N1s spectrum after single annealing. The only difference was the appearance of an additional signal at BE = 402.8 eV, which may suggest the presence of nitrogen admixtures of the NO_x type in the TiO_2 lattice.[3,19,49] The BE can be attributed to NO_2^- nitrite ions, i.e., the formation of N−O bonds. In addition to this additional peak, signals were identified that correspond to the bonds: Ti−N (396.5 eV, substitution nitrogen), Ti−O−N (398.7 eV, interstitial nitrogen), and chemisorbed nitrogen on the nanotube surface (400.4 eV). The characteristic shape of the XPS-VB spectrum with a "gap" of about 3.2 eV did not change significantly in relation to the single-annealed sample. Similar to the first annealing at 450 °C, the share of nitrogen effectively introduced into the anatase network as a permanent dopant (substitute nitrogen, interstitial nitrogen, NO_x) was at a level of 56%, with a contribution of Ti−N bonds of about 12%. The XPS in situ tests showed that the process of plasma nitriding together with thermal treatment makes it possible to modify the electronic structure of TiO_2 by the appearance of interstitial impurities or mixed states containing both interstitial and substitutional impurities. Such results will have a different impact on the photocurrent response of the tested systems.

Figure 5 shows the UV−vis spectra for the produced materials and the Tauc diagrams on the basis of which the optical bandgap energy (E_g) was determined using the

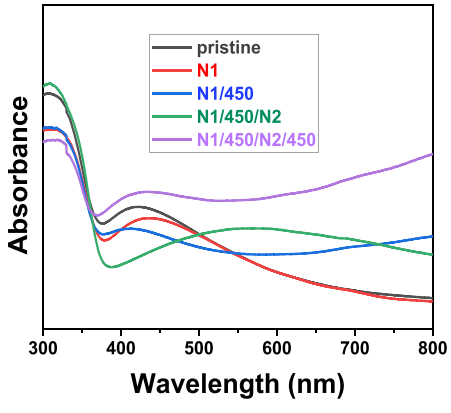

Figure 5. UV−vis DRS spectra of all investigated samples.

https://doi.org/10.1021/acsanm.3c01278
ACS Appl. Nano Mater. 2023, 6, 10351−10364

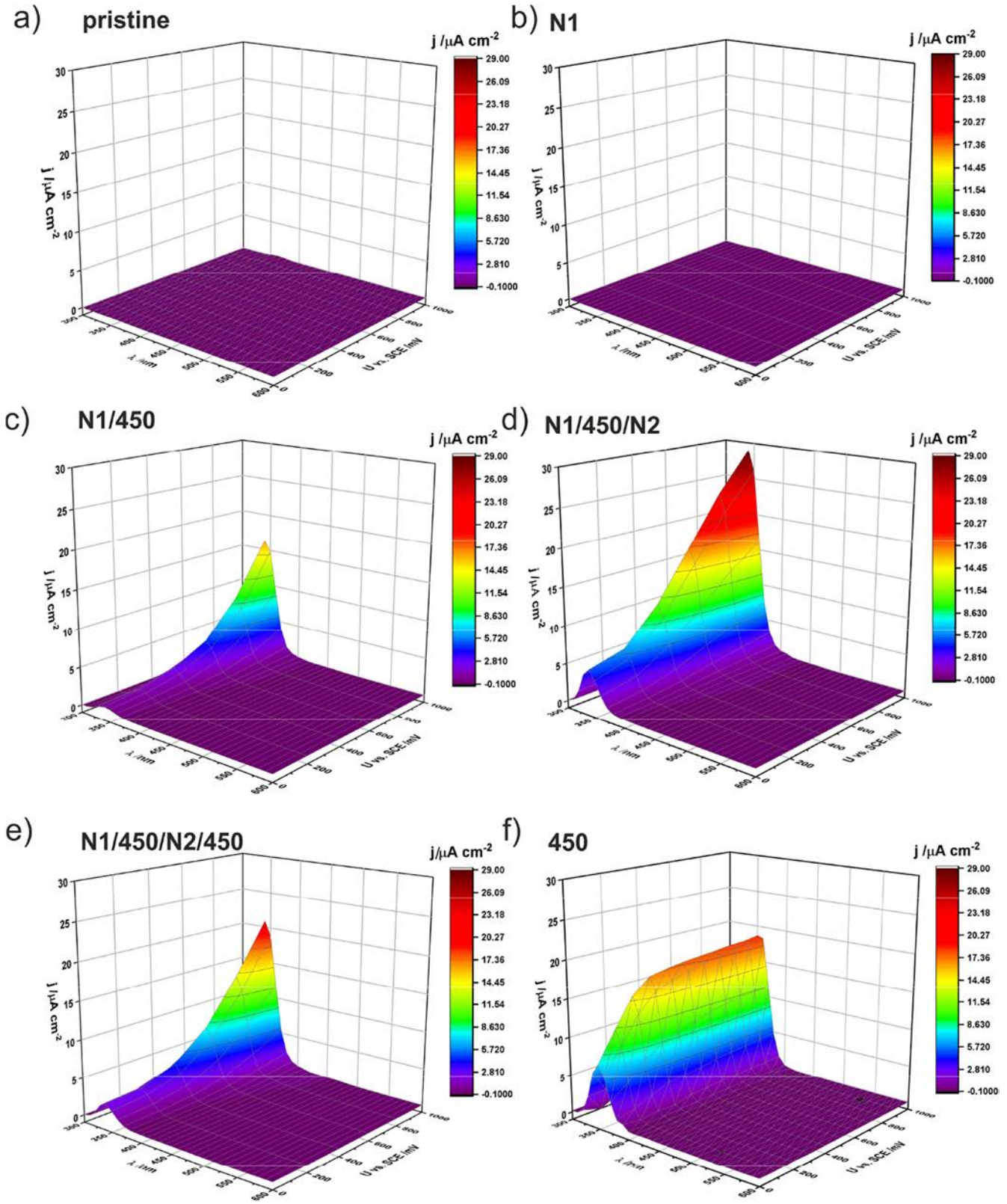

Figure 6. Photocurrent density as a function of incident light wavelength and applied potential, recorded for pristine nanotubes (a), nitrided—N1 (b), annealed at 450 °C—N1/450 (c), nitrided—N1/450/N2 (d), annealed at 450 °C—N1/450/N2/450 (e), and only annealed at 450 °C as the reference data—450 (f). The surface functionalization of the TiO_2 nanotubes was performed under UHV conditions.

Kubelka−Munk method (Figure S2 in the Supporting Information). The UV−vis data (Figure 5) show that the absorbance of nitrided nanotubes annealed at 450 °C in the visible light region was larger than that of the tubes in the initial state (pristine). The larger light absorbance in the visible region resulted from the appearance of nitrogen atoms in the TiO_2 structure and changes in the electronic structure of the oxide,[15,29] as confirmed by the XPS studies. Nevertheless,

https://doi.org/10.1021/acsanm.3c01278
ACS Appl. Nano Mater. 2023, 6, 10351−10364

some dependencies on the UV−vis spectra can be noticed. First, the spectra for pristine nanotubes and those nitrided once (N1) are similar in character across the entire range of wavelengths. The only difference is a shift in the broad maxima of the TiO_2 absorption peak, from about 425 to about 440 nm. Second, annealing at 450 °C led to a change in the nature of the spectra for individual samples (N1/450, N1/450/N2/450) and to an increase in light absorption above 550 nm. This is related to the transformation of the structure of the TiO_2 nanotubes, from an amorphous form into a crystalline form—anatase—and probably to the appearance of oxygen vacancies as a result of the plasma-nitriding process and annealing in vacuum (presence of Ti^{3+} ions).[15,59,61] Third, the shape of the spectrum for the sample twice nitrided and once annealed (N1/450/N2) differs from the others. It can be clearly seen that the absorbance range for this sample has extended from about 380 to 700 nm, with a maximum at about 550 nm. This behavior is directly related to the observed structural changes in TiO_2, the process of doping with nitrogen—and particularly the interstitial position[13,15,42,43]—as well as morphological factors related to light scattering on the surface of nanotubes of a certain length.[22] The observed increase in the absorption of UV light to the visible range in the case of the nitrided samples is undoubtedly related to the doping process, where nitrogen atoms imply the formation of new, mixed N 2p energy levels near the valence band, and where non-stoichiometric oxides (Ti^{3+}) can modify the electronic structure of TiO_2, creating a donor level below the conduction band corresponding to the states of oxygen vacancies.[15,59−61] In addition, the oxygen vacancies are associated with a reduction in the O^{2-} dianion to the O^- anion in the anatase structure, resulting in the appearance of "volumetric centers" in the vicinity of Ti^{4+}, which absorb light in the range from 550 to 800 nm; subsurface centers from 430 to 550 nm; and surface centers below 430 nm, as was noticed by Zawadzki[62] and summarized in Schneider's work.[63] These effects can be clearly observed in the recorded UV−vis spectra where, for the double-annealed and nitrided sample, three peaks can be seen at ∼430, 600, and 700 nm and, for the double-nitrided and single-annealed sample, where the maximum is at 550 nm. The migration of photogenerated holes to surface and subsurface sites is therefore possible and affects the photocatalytic activity of the resulting photoanodes in the visible light range, where the surface plays a key role.[62] These factors can lead to a reduction in the bandgap energy (E_g), although this effect has not been demonstrated using Kubelka−Munk calculations (see Figure S2). The estimated optical bandgap energy is slightly larger than for the XPS-VB approximation and varies from 3.31 to 3.41 eV. Nevertheless, slight differences can be observed in the double-nitrided and single-annealed sample (N1/450/N2) in the XPS measurements. The differences in the E_g determined using the two methods result from their depth resolution and the physical basis of the techniques themselves. In the case of XPS, we record surface changes, because the inelastic mean free path of electrons in TiO_2 is only about 2.2 nm, calculated on the basis of the TPP-2M formula,[64] with an X-ray source excitation energy of 1486.6 eV. However, in the case of UV−vis measurements in a wavelength range of 300−800 nm, the light penetrates the nanotubes much deeper due to the open porosity of the nanostructures.[65,66] Moreover, our previous work shows that nitrogen introduced into the crystallographic structure of nanotubes annealed at 450 °C is located mainly in the near-surface zones of <10 nm; it is then concentrated deep into the nanotubes at a constant level of about 0.5 at %.[24] Nevertheless, our data are consistent with the literature data, where Wang et al. calculated the bandgap from the density of the electron states (DOS) as 3.42 eV. Other experimental data, though, have shown a gap of 3.26 eV.[15] Another reason for these divergences may be related to the change in the chemical composition of TiO_2 after it is doped with nitrogen, which was observed by Preethi et al.[40] Using UPS spectroscopy, they found that there was a change in the position of the Fermi level at different concentrations of nitrogen doped into the TiO_2 structure and that this affected both the number of defects caused by the presence of Ti^{3+} ions and the density of N 2p states. An increase in nitrogen concentration led to a decrease in the bandgap energy (E_g) as the EF band shifted to CB, though this occurred only at the optimal nitrogen content in the TiO_2 lattice. As the nitrogen concentration continued to increase, the Fermi level moved away from the edge of the conduction band, and then the density of defective Ti^{3+} states reached the maximum saturation level, meaning that it did not influence the width of the bandgap, which is affected only by the density of N 2p states near the valence level.[40,41] Therefore, the change in the density of N 2p states strictly depends on the concentration of nitrogen in the TiO_2 structure,[14,40,46,67] which can be controlled by the correct application of thermochemical treatments under UHV conditions. All these changes led to slightly different bandgap energy results when determined using various measurement methods.

Photocurrent density maps recorded for individual nitrided and in situ annealed samples in relation to the pristine sample are shown in Figure 6. Figure 6a clearly shows that the anodic TiO_2 nanotubes whose electronic structure was unmodified showed an almost insignificant photoresponse in the UV−vis range. The maximum photocurrent density was <0.2 $\mu A \cdot cm^{-2}$ for the wavelength λ = 360 nm. This effect is related to the structure of the nanotubes immediately after the anodization process, which is amorphous. Then, most of the photocurrent response is probably generated at the bottom of the nanotubes (height about 1 μm), with only a negligible contribution of the walls themselves due to the large number of defects they contain, which act as electron traps, leading to a high recombination rate of electron−hole pair carriers.[65,66] After the introduction of nitrogen into the amorphous structure (N1), no significant changes were observed in the photocurrent maps (Figure 6b), despite the observed shift in the maximum light absorption peak for TiO_2. The maximum photocurrent density was at a similar level < 0.2 $\mu A \cdot cm^{-2}$. As can be seen from the above results, despite the presence of nitrogen atoms in the amorphous structure of TiO_2, TiO_2 did not exhibit any photoactivity. Only annealing the sample at 450 °C for 2 h (N1/450) resulted in a significant increase in the maximum photocurrent density, up to about 16.0 $\mu A \cdot cm^{-2}$ for λ = 350 nm (UV range), which is associated with a change in the structure of TiO_2 from amorphous to crystalline—anatase—and the appearance of admixtures such as substitution nitrogen (Ti−N) and interstitial nitrogen (Ti−O−N) in the TiO_2 lattice (Figure 6c).[1,17,27,33,52] Another nitriding process (N1/450/N2), this time by introducing nitrogen into the crystal structure of TiO_2, led to another increase in the photocurrent maximum at the same wavelength, up to a value of about 30.0 $\mu A \cdot cm^{-2}$ (Figure 6d). This phenomenon is mainly due to the presence of interstitial nitrogen but with a different bond configuration between Ti, N, and O in the nanotube structure (Ti−N−O). The appearance of extra

https://doi.org/10.1021/acsanm.3c01278
ACS Appl. Nano Mater. 2023, 6, 10351−10364

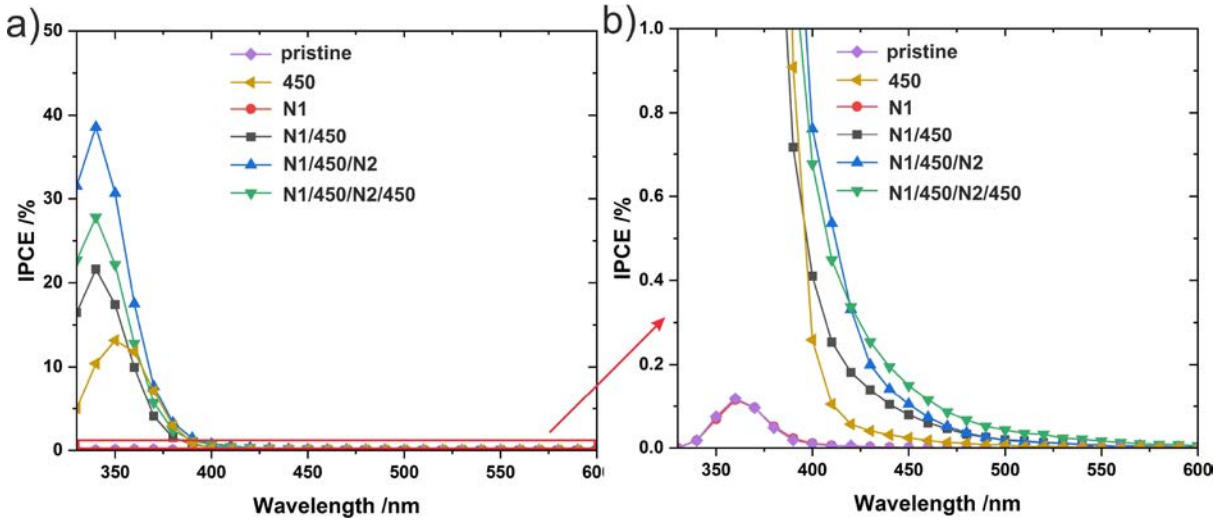

Figure 7. (a and b) IPCE spectra at U = 1 V vs SCE for all the photo-anodes studied in the UV−vis range.

nitrogen in the TiO_2 lattice affects its electronic structure, leading to a change in its light absorption properties. This is related to the partial transfer of electrons from N to Ti^{4+} and the resulting increase in the electron density on Ti^{4+} ($Ti^{(4-\sigma)+}$) due to the lower electronegativity of nitrogen compared to that of oxygen.[11,13,17,43,67] In addition, the appropriate level of N doping ensures a favorable separation of photogenerated electron−hole pairs, which leads to higher photocatalytic activity. In our case, that level was about 1.9 at %. Note here that the recombination of photogenerated electrons/holes can occur too quickly during charge transport when there is too much doped nitrogen. Our results showed a good correlation with the XPS and UV−vis absorbance spectroscopy data (see Figures 4 and 5). The second annealing after secondary nitriding (N1/450/N2/450) contributed to a decrease in the maximum photocurrent density for λ = 350 nm to about 20 $\mu A \cdot cm^{-2}$ (Figure 6e). This decrease in current density may be related to a reorganization of the types of bonds in the TiO_2 lattice under the influence of the thermal treatment, where we again observed characteristic Ti−N (substitution nitrogen) and Ti−O−N bonds (interstitial nitrogen). Moreover, after the second annealing, the presence of Ti^{3+} was detected, resulting in the appearance of oxygen holes on the surface of the nanotubes. All these factors are desirable to achieve high photoactivity by changing the electronic structure of TiO_2. In this case, according to the literature data, theoretical DFT calculations show that this kind of nitrogen doping leads to the generation of additional states, i.e., localized N 2p levels above the valence band maximum and Ti^{3+} 3d states below the conduction band.[61,62] Therefore, it can be assumed that, for the photoanode N1/450/N2/450, the PEC activity in the UV−vis range comes from N 2p levels near the valence band, while oxygen vacancies and associated Ti^{3+} species act as recombination centers for the photoinduced electrons and holes. They reduce the photocatalytic activity but, on the other hand, contribute to the absorption of visible light,[15,36,45,48,61] as can be seen in the UV−vis spectra. The photocurrent measurements also suggest that doping with nitrogen followed by thermal treatment at 450 °C (2 h) results in a significant improvement in optical absorption compared to the unannealed photoanodes (see Figure 6f). Linear sweep voltammetry (LSV) curves recorded in darkness and under illumination which are shown in Figure S3 (Supporting Information) also confirmed that the thermal treatment of the samples at 450 °C and UHV nitriding is crucial for their promising photoresponse. The second nitriding (N1/450/N2) not only results in a noticeable increase in photocurrents observed but also shifts the onset potential to slightly more negative values. Moreover, the fragments of chronoamperometric curves shown in Figure S4 (Supporting Information) confirm the stability of the photoanodes understood as their resistance to additional electrochemical oxidation during anodic polarization indicated by low dark current values. Additional measurements based on chronoamperometric curves which were recorded under 30 min irradiation with a Xe lamp (at the maximum λ = 350 nm) for all studied samples showed a positive effect of nitrogen doping along with thermal treatment (Figure S5 in the Supporting Information). Although we observe a gradual decrease in the current density during the first minutes of irradiation, which may suggest some instability of the produced photoanodes, it appears that the obtained results are promising. The explanation of these instabilities requires further research and perhaps further optimization of the nitriding process under UHV conditions. Nevertheless, the course of chronoamperometric curves is typical, where at the beginning we observe a step increase in photocurrents after switching on the light and then its slow decrease. Perhaps it is related to the change in the mechanism of surface recombination. When the light is turned on, photogenerated holes in the titanium oxide diffuse to the surface of the nanotubes, causing appropriately high photocurrents. These holes can then be trapped by surface states, resulting in their accumulation as efficient recombination sites for the generated electrons. As a consequence, this leads to a decrease in the measured photocurrent values,[68] which was also shown by earlier measurements of photocurrent maps, see Figure 6. These measurements clearly show that the doping method, and thus the surface chemical composition, plays a key role. It may be related to the different participation of chemisorbed nitrogen on the TiO_2 NT surface, the amount of which decreases each time after the heating process at 450 °C, as confirmed by the XPS investigations. This nitrogen is attached to the surface of the TiO_2 nanotubes only through interactions such as dipole−dipole and van der Waals forces.[1,43]

https://doi.org/10.1021/acsanm.3c01278
ACS Appl. Nano Mater. 2023, 6, 10351−10364

Table 2. IPCE Values Observed for All Studied Samples at Three Different Wavelengths The maximum values are in bold.

sample	IPCE at 350 nm/%	IPCE at 400 nm/%	IPCE at 450 nm/%
pristine	0.07	0.01	0.001
450	13.18	0.26	0.024
N1	0.07	0.01	0.001
N1/450	17.42	0.41	0.079
N1/450/N2	**30.64**	**0.76**	0.105
N1/450/N2/450	22.16	0.68	**0.150**

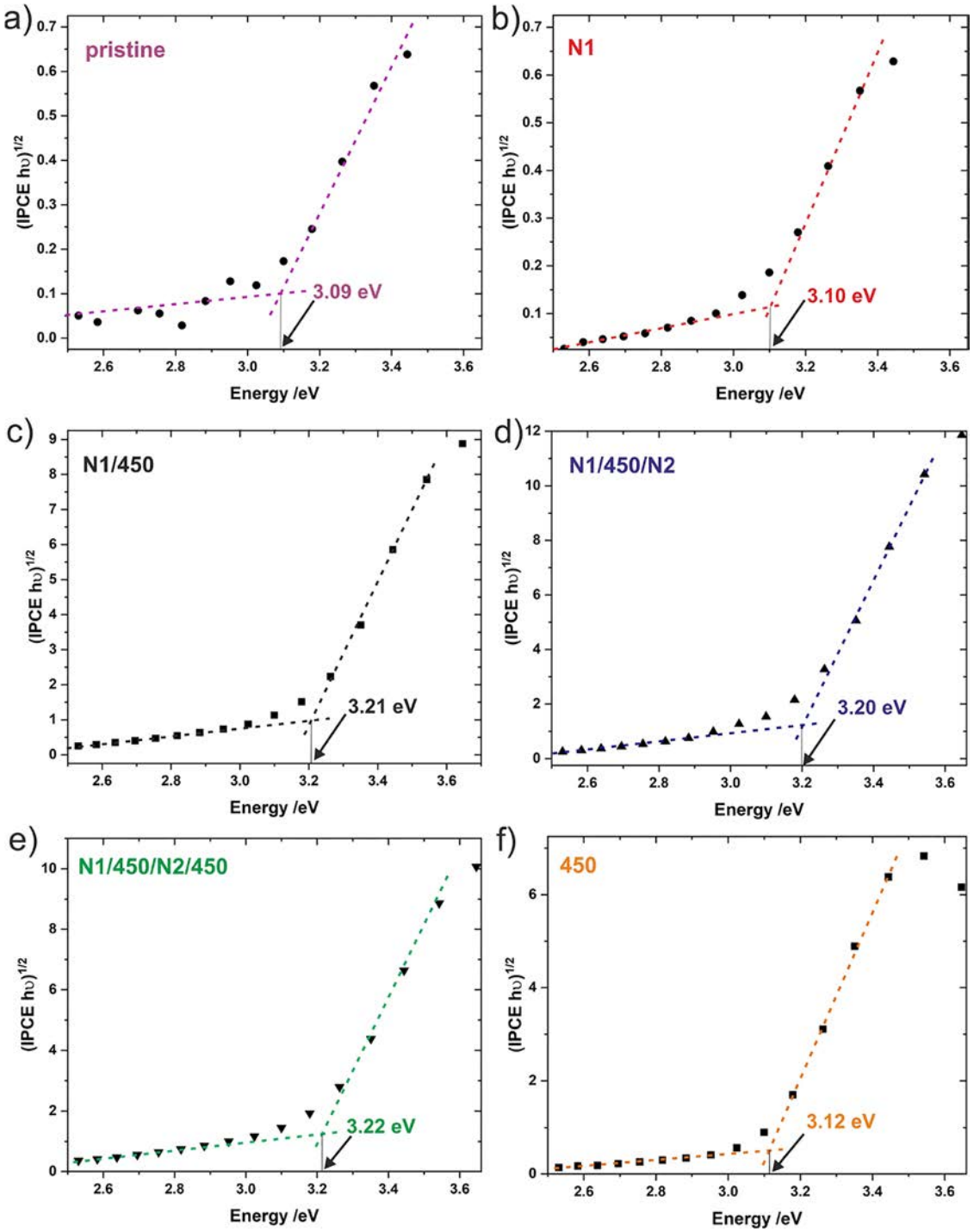

Figure 8. (a–f) (IPCE $h\nu$)$^{0.5}$ vs $h\nu$ plots (Tauc plots) together with estimated E_g for annealed and nitrided samples.

Subsequently, the IPCE values (photon current efficiency) at 1 V vs SCE were collected and calculated, as shown in Figure 7a,b. The spectra confirm that the most significant photoconversion was obtained in the UV range regardless of

https://doi.org/10.1021/acsanm.3c01278
ACS Appl. Nano Mater. 2023, 6, 10351−10364

the sample type. The highest IPCE values were obtained for the sample twice nitrided and once annealed in situ (N1/450/N2). This significant improvement in photoactivity was related to obtaining a stable crystalline TiO_2 structure after annealing—anatase—as well as a change in the electronic structure of the oxide, where the N 2p states became dominant near the Fermi level; these are discrete energy levels at the upper edge of the valence band, leading to a loss in strong hybridization between Ti 3d and O 2p.[46] It is known that, for pure TiO_2, the O 2p states dominate at the top of the valence band and the Ti 3d states dominate at the bottom of the conduction band, where the energy gap comes from the splitting of the Ti 3d and O 2p hybridization bands near the Fermi level (minimal photoactivity).[3,40,59,60] The available literature data indicate that even a small amount of N impurity in the O sites in a TiO_2 lattice can cause a change in the structure of the edge of the valence band near the Fermi level. The N 2p states then dominate over the O 2p states, weakening the strong hybridization between Ti 3d and O 2p. This results in, among other things, a reduced bandgap (see Figure 4p).[40,46] Thus, the combination of the N-doping process and the presence of O vacancies resulting from annealing under UHV conditions[35,61] is responsible for the increased efficiency of the IPCE, which is a measure of the ratio of photon (converted to electron transfer rate) to incident photon velocity as a function of photon wavelength (see Figure 7a). A detailed inspection of the IPCE spectra revealed that the combination of two nitriding processes and annealing at 450 °C (N1/450/N2) enhanced the photoconversion of TiO_2 NTs in the visible range (Figure 7b). Although there are no well-defined maxima in the wavelength range from 450 to 800 nm, as there are in the UV−vis spectra, it can be seen that the IPCE gain gradually increased with the wavelength of the incident light. It is evident that the shift toward visible light was greatest for the double-nitrided sample annealed once (N1/450/N2) or twice (N1/450/N2/450). This was related to the appearance of nitrogen in the TiO_2 lattice as interstitial (Ti−N−O, Ti−O−N) or substitutional (Ti−N) impurities. Table 2 summarizes the IPCE performance results for various wavelengths at 350, 400, and 450 nm for all studied samples.

Again, it is clear that the best PEC performance in the UV range is achieved for the photoanode nitrided twice and annealed (N1/450/N2). Second annealing after the second nitriding results (N1/450/N2/450) in worsening of PEC activity in the UV range but further increases the IPCE in the visible range.

Taking these results into account, we can conclude that, by controlling the parameters of nitriding and by annealing under UHV conditions, we are able to cause the appearance of various forms of nitrogen admixtures, which ultimately affect the photocatalytic properties of the TiO_2 nanotubes.[69]

Figure 8a−f shows graphs of $(\text{IPCE } h\nu)^{0.5}$ vs $h\nu$ (Tauc plots) for the tested samples, plotted in order to determine the energy bandgap for these in the photoelectrochemical measurements. As for the Kubelka−Munk calculations based on the diffuse reflection method (DRS), the effects expected related to a change in the bandgap width (E_g) were not demonstrated. Nevertheless, in this case, for the method used, the results were more consistent with the XPS-VB data. The bandgap energy changed from 3.09 eV for TiO_2 NTs in the initial state (pristine) to 3.22 eV for the N1/450/N2/450 sample. The bandgap energy determined for the samples annealed at 450 °C corresponds to the values for anatase (3.2 eV[69]), which, among other things, determines the photocatalytic properties of the produced materials in the UV range.

Taking all the above considerations into account, it can be concluded that many independent factors simultaneously cause subtle changes in the electronic structure of TiO_2 nanotubes after nitriding. In particular, these changes are observable in the surface and subsurface regions, as shown schematically in Figure 9.

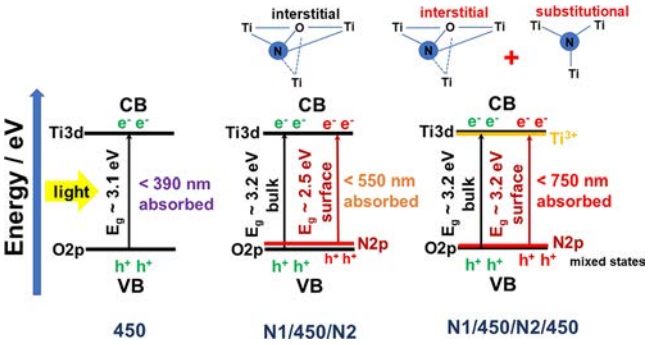

Figure 9. Scheme showing the change in the properties of the electronic structure of nitrogen-doped titanium dioxide in the form of nanotubes under the influence of heat-chemical treatment under UHV conditions based on spectrophotoelectrochemical, UV−vis, and XPS data.

CONCLUSIONS

By using plasma nitriding in combination with the high-temperature treatment of TiO_2 nanotubes, it was possible to produce active photoanodes in the UV−vis light range. By alternately controlling the process of nitriding and annealing at 450 °C, it was possible to successfully incorporate nitrogen into the interstitial or substitutional positions of atoms in the crystal structure of the TiO_2 nanotubes. This method of functionalizing TiO_2 nanotubes under UHV conditions did not lead to significant morphological changes. The most significant changes occurred in the crystallographic and electronic structure of the TiO_2 NTs, in particular for the N1/450/N2 and N1/450/N2/450 photoanodes. For these samples, evident changes were observed in the light absorption properties in the UV−vis range, where there was a shift toward visible light. The maximum photocurrent densities of ∼30.0 and ∼20.0 $\mu A \cdot cm^{-2}$ were also recorded for these, respectively. Our measurements also showed that the last stage of thermo-chemical treatment in 450 °C led to a reduction in the amount of nitrogen chemisorbed to the surface of the nanotubes. The doped anatase structure was the main source of the photoresponse of the tested materials in the UV light range, and so no significant changes in the TiO_2 bandgap were found. The estimated E_g values, regardless of the measurement methods used, were close to the values for pure anatase 3.2 eV. The only exception was the double-nitrided and once-annealed sample (N1/450/N2), where a certain reduction in E_g was observed, associated with the appearance of interstitial nitrogen in the TiO_2 lattice. This caused mixed N 2p states to form near the valence band, with an optimal concentration of nitrogen in the sample. In addition, the regular morphology of the nanotubes and their arrangement toward the metallic substrate (Ti) ensured specific light scattering and absorption, which also affected the photoresponse generated in the photoanodes obtained.

https://doi.org/10.1021/acsanm.3c01278
ACS Appl. Nano Mater. 2023, 6, 10351−10364

■ ASSOCIATED CONTENT

Supporting Information

The Supporting Information is available free of charge at https://pubs.acs.org/doi/10.1021/acsanm.3c01278.

XRD patterns of nitrided and annealed materials; Tauc plots—determination of the optical bandgap (E_g); LSV curves of nitride and annealed samples; and chronoamperometric curves based on measurements of photocurrent maps or continuous Xe lamp irradiation (PDF)

■ AUTHOR INFORMATION

Corresponding Author

Marcin Pisarek − *Institute of Physical Chemistry, Polish Academy of Sciences, 01-224 Warsaw, Poland*; orcid.org/0000-0002-7424-5954; Phone: +48 22 343 3325; Email: mpisarek@ichf.edu.pl; Fax: +48 22 343 33 33

Authors

Mirosław Krawczyk − *Institute of Physical Chemistry, Polish Academy of Sciences, 01-224 Warsaw, Poland*

Magdalena Gurgul − *Faculty of Chemistry, Jagiellonian University in Kraków, 30-387 Kraków, Poland*

Leszek Zaraska − *Faculty of Chemistry, Jagiellonian University in Kraków, 30-387 Kraków, Poland*

Krzysztof Bieńkowski − *Laboratory of Molecular Research for Solar Energy Innovations, Centre of New Technologies University of Warsaw, 02-097 Warsaw, Poland*

Marcin Hołdyński − *Institute of Physical Chemistry, Polish Academy of Sciences, 01-224 Warsaw, Poland*

Renata Solarska − *Laboratory of Molecular Research for Solar Energy Innovations, Centre of New Technologies University of Warsaw, 02-097 Warsaw, Poland*

Complete contact information is available at: https://pubs.acs.org/10.1021/acsanm.3c01278

Notes

The authors declare no competing financial interest.

■ ACKNOWLEDGMENTS

This work was financially supported by the Institute of Physical Chemistry PAS—Laboratory of Surface Analysis. R.S. and K.B. gratefully acknowledge the financial support of the National Center for Research and Development (project number NOR/POLNOR/HERA/0043/2019).

■ REFERENCES

(1) Ansari, S. A.; Mansoob Khan, M.; Ansari, M. O.; Cho, M. H. Nitrogen-doped titanium dioxide (N-doped TiO_2) for visible light photocatalysis. *New J. Chem.* **2016**, *40*, 3000−3009.

(2) Wang, M.; Ioccozia, J.; Sun, L.; Lin, C.; Lin, Z. Inorganic-modified semiconductor TiO_2 nanotube arrays for photocatalysis. *Energy Environ. Sci.* **2014**, *7*, 2182−2202.

(3) Natarajan, T. S.; Mozhiarasi, V.; Tayade, R. J. Nitrogen Doped Titanium Dioxide (N-TiO_2): Synopsis of Synthesis Methodologies, Doping Mechanisms, Property Evaluation and Visible Light Photocatalytic Applications. *Photochem* **2021**, *1*, 371−410.

(4) Fadlallah, M. M. Magnetic, electronic, optical, and photocatalytic properties of nonmetal and halogen-doped anatase TiO_2 nanotubes. *Phys. E* **2017**, *89*, 50−56.

(5) Nah, Y.-C.; Paramasivam, I.; Schmuki, P. Doped TiO_2 and TiO_2 Nanotubes: Synthesis and Applications. *ChemPhysChem* **2010**, *11*, 2698−2713.

(6) Andoshe, D. M.; Yim, K.; Sohn, W.; Kim, C.; Kim, T. L.; Kwon, K. C.; Hong, K.; Choi, S.; Moon, C. W.; Hong, S.-P.; Han, S.; Jang, H. W. One-pot synthesis of sulfur and nitrogen codoped titanium dioxide nanorod arrays for superior photoelectrochemical water oxidation. *Appl. Catal., B* **2018**, *234*, 213−222.

(7) Park, J.; Lee, S.; Lee, T. H.; Kim, C.; Jun, S. E.; Baek, J. H.; Kim, J. Y.; Lee, M. G.; Ahn, S. H.; Jang, H. W. Regulating the surface of anion-doped TiO_2 nanorods by hydrogen annealing for superior photoelectrochemical water oxidation. *Nano Convergence* **2022**, *9*, 33.

(8) Fujishima, A.; Honda, K. Electrochemical Photolysis of Water at a Semiconductor Electrode. *Nature* **1972**, *238*, 37−38.

(9) Du, S.; Lian, J.; Zhang, F. Visible Light-Responsive N-Doped TiO_2 Photocatalysis: Synthesis, Characterizations, and Applications. *Trans. Tianjin Univ.* **2022**, *28*, 33−52.

(10) Kim, H.-I.; Monllor-Satoca, D.; Kim, W.; Choi, W. N-doped TiO_2 nanotubes coated with a thin TaO_xN_y layer for photoelectrochemical water splitting: dual bulk and surface modification of photoanodes. *Energy Environ. Sci.* **2015**, *8*, 247−257.

(11) Zhang, X.; Zhou, J.; Gu, Y.; Fan, D. Visible-Light Photocatalytic Activity of N-Doped TiO_2 Nanotube Arrays on Acephate Degradation. *J. Nanomater.* 2015, *2015*, 527070 (6 pages), DOI: 10.1155/2015/527070.

(12) Tang, H.; Prasad, K.; Sanjinbs, R.; Schmid, P. E.; Levy, F. Ellectrical and optical properties of TiO_2 anatase thin films. *J. Appl. Phys.* **1994**, *75*, 2042−2047.

(13) Wang, Y.; Zhu, L.; Ba, N.; Gao, F.; Xie, H. Effects of NH_4F quantity on N-doping level. photodegradation and photocatalytic H_2 production activities of N-doped TiO_2 nanotube array films. *Mater. Res. Bull.* **2017**, *86*, 268−276.

(14) Mahy, J. G.; Cerfontaine, V.; Poelman, D.; Devred, F.; Gaigneaux, E.M.; Heinrichs, B.; Lambert, S. D. Highly Efficient Low-Temperature N-Doped TiO_2 Catalysts for Visible Light Photocatalytic Applications. *Materials* 2018, *11*, 584(20 pages), DOI: 10.3390/ma11040584.

(15) Wang, J.; Tafen De, N.; Lewis, J. P.; Hong, Z.; Manivannan, A.; Zhi, M.; Li, M.; Wu, N. Origin of Photocatalytic Activity of Nitrogen-Doped TiO_2 Nanobelts. *J. Am. Chem. Soc.* **2009**, *131*, 12290−12297.

(16) (a) Di Valentin, C.; Pacchioni, G.; Selloni, A. Origin of the different photoactivity of N-doped anatase and rutile TiO_2. *Phys. Rev. B* **2004**, *70*, 085116-1−085116-4. (b) Rumaiz, A. K.; Woicik, J. C.; Cockayne, E.; Lin, H. Y.; Jaffari, G. H.; Shah, S. I. Oxygen vacancies in N doped anatase: Experiment and first-principles calculations. *Appl. Phys. Lett.* **2009**, *95*, 262111.

(17) Cong, Y.; Zhang, J.; Chen, F.; Anpo, M. Synthesis and Characterization of Nitrogen-Doped TiO_2 Nanophotocatalyst with High Visible Light Activity. *J. Phys. Chem. C* **2007**, *111*, 6976−6982.

(18) He, Z.; Que, W.; He, Y.; Hu, J.; Chen, J.; Asif Javed, H. M.; Ji, Y.; Li, X.; Fei, D. Electrochemical behavior and photocatalytic performance of nitrogen-doped TiO_2 nanotubes arrays powders prepared by combining anodization with solvothermal process. *Ceram. Int.* **2013**, *39*, 5545−5552.

(19) Huang, J.-R.; Tan, X.; Yu, T.; Hu, W.-L.; Zhao, L.; Liu, H.; Zhang, L.; Zou, Y.-L. N-Doped TiO_2/$SrTiO_3$ Heterostructured Nanotubes for High-Efficiency Photoelectrocatalytic Properties under Visible-Light Irradiation. *ChemElectroChem* **2015**, *2*, 1174−1181.

(20) Tang, P.; Li, X.; Xie, C.; Xiao, X. Effect of Titanium Matrix Structure on Growth Morphology of Anodized TiO_2 Nanotube Arrays for Applications in Photoelectrochemical Performances. *ACS Appl. Nano Mater.* **2023**, *6*, 410−420.

(21) Harynski, Ł.; Czylkowski, D.; Hrycak, B.; Karczewski, J.; Gumieniak, J.; Kramek, A.; Ryl, J.; Grochowska, K.; Dors, M.; Siuzdak, K. Nitrogen plasma-induced crystallization of anodic TiO_2 nanotubes for solar photoelectrochemistry. *Appl. Surf. Sci.* 2023, *615*, 156472(9 pages), DOI: 10.1016/j.apsusc.2023.156472.

(22) Macak, J. M.; Ghicov, A.; Hahn, R.; Tsuchiya, H.; Schmuki, P. Photoelectrochemical properties of N-doped self-organized titania nanotube layers with different thicknesses. *J. Mater. Res.* **2006**, *21*, 2824−2828.

(23) Roguska, A.; Pisarek, M.; Belcarz, A.; Marcon, L.; Holdynski, M.; Andrzejczuk, M.; Janik-Czachor, M. Improvement of the biofunctional properties of TiO_2 nanotubes. *Appl. Surf. Sci.* **2016**, *388*, 775−785.
(24) Pisarek, M.; Krawczyk, M.; Holdynski, M.; Lisowski, W. Plasma Nitriding of TiO_2 Nanotubes: N Doping in Situ Investigations Using XPS. *ACS Omega* **2020**, *5*, 8647−8658.
(25) Jarosz, M.; Syrek, K.; Kapusta-Kołodziej, J.; Mech, J.; Małek, K.; Hnida, K.; Łojewski, T.; Jaskuła, M.; Sulka, G. D. Heat Treatment Effect on Crystalline Structure and Photoelectrochemical Properties of Anodic TiO_2 Nanotube Arrays Formed in Ethylene Glycol and Glycerol Based Electrolytes. *J. Phys. Chem. C* **2015**, *119*, 24182−24191.
(26) Chen, C. L.; Dong, C.-L.; Chen, C.-H.; Wu, J.-W.; Lu, Y.-R.; Lin, C.-J.; Liou, S. Y. H.; Tseng, C.-M.; Kumar, K.; Wei, D.-H.; Guo, J.; Chou, W.-C.; Wu, M.-K. Electronic properties of free-standing TiO_2 nanotube arrays fabricated by electrochemical anodization. *Phys. Chem. Chem. Phys.* **2015**, *17*, 22064−22071.
(27) Mazierski, P.; Nischk, M.; Gołkowska, M.; Lisowski, W.; Gazda, M.; Winiarski, M. J.; Klimczuk, T.; Zaleska-Medynska, A. Photocatalytic activity of nitrogen doped TiO_2 nanotubes prepared by anodic oxidation: The effect of applied voltage, anodization time and amount of nitrogen dopant. *Appl. Catal., B* **2016**, *196*, 77−88.
(28) Yan, J.; Zhou, F. TiO_2 nanotubes: Structure optimization for solar cells. *J. Mater. Chem.* **2011**, *21*, 9406−9418.
(29) Lai, Y.-K.; Huang, J.-Y.; Zhang, H.-F.; Subramaniam, V.-P.; Tang, Y.-X.; Gong, D.-G.; Sundar, L.; Sun, L.; Chen, Z.; Lin, C.-J. Nitrogen-doped TiO_2 nanotube array films with enhanced photocatalytic activity under various light sources. *J. Hazard. Mater.* **2010**, *184*, 855−863.
(30) Roy, P.; Berger, S.; Schmuki, P. TiO_2 Nanotubes: Synthesis and Applications. *Angew. Chem., Int. Ed.* **2011**, *50*, 2904−2939.
(31) Divyasri, Y. V.; Reddy, N. L.; Lee, K.; Sakar, M.; Rao, V. N.; Venkatramu, V.; Shankar, M. V.; Reddy, N. Ch. G. Optimization of N doping in TiO_2 nanotubes for enhanced solar light mediated photocatalytic H_2 production and dye degradation. *Environ. Pollut.*2021, *269* 116170(12 pages), DOI: 10.1016/j.envpol.2020.116170.
(32) Yuan, B.; Wang, Y.; Bian, H.; Shen, T.; Wu, Y.; Chen, Z. Nitrogen doped TiO_2 nanotube arrays with high photoelectrochemical activity for photocatalytic applications. *Appl. Surf. Sci.* **2013**, *280*, 523−529.
(33) Siuzdak, K.; Szkoda, M.; Sawczak, M.; Lisowska-Oleksiak, A. Novel nitrogen precursors for electrochemically driven doping of titania nanotubes exhibiting enhanced photoactivity. *New J. Chem.* **2015**, *39*, 2741−2751.
(34) Bonelli, T. S.; Pereyra, I. Low temperature RF plasma nitriding of self-organized TiO_2 nanotubes for effective bandgap reduction. *Appl. Surf. Sci.* **2018**, *442*, 239−244.
(35) Le, P.H.; Hieu, L.T.; Lam, T.-N.; Hang, N.T.N.; Truong, N.V.; Tuyen, L.T.C.; Phong, P.T.; Leu, J. Enhanced Photocatalytic Performance of Nitrogen-Doped TiO_2 Nanotube Arrays Using a Simple Annealing Process. *Micromachines* 2018, *9*, 618(13 pages), DOI: 10.3390/mi9120618.
(36) Liu, X.; Liu, Z.; Zheng, J.; Yan, X.; Li, D.; Chen, S.; Chu, W. Characteristics of N-doped TiO_2 nanotube arrays by N_2-plasma for visible light-driven photocatalysis. *J. Alloys Compd.* **2011**, *509*, 9970−9976.
(37) Rojviroon, T.; Rojviroon, O.; Sirivithayapakorn, S.; Angthong, S. Application of TiO_2 nanotubes as photocatalysts for decolorization of synthetic dye wastewater. *Water Resour. Ind.* 2021, *26*, 100163(10 pages), DOI: 10.1016/j.wri.2021.100163.
(38) Meng, Q.-Q.; Wang, J.-G.; Xie, Q.; Dong, H.-Q.; Li, X.-N. Water splitting on TiO_2 nanotube arrays. *Catal. Today* **2011**, *165*, 145−149.
(39) Chen, B.; Hou, J.; Lu, K. Formation Mechanism of TiO_2 Nanotubes and Their Applications in Photoelectrochemical Water Splitting and Supercapacitors, H_2 production, pure TiO_2 nanotubes. *Langmuir* **2013**, *29*, 5911−5919.
(40) Preethi, L. K.; Antony, R. P.; Mathews, T.; Walczak, L.; Gopinath, Ch. S. A Study on Doped Heterojunctions in TiO_2 Nanotubes: An Efficient Photocatalyst for Solar Water Splitting. *Sci. Rep.* 2017, *7*, 14314(15 pages), DOI: 10.1038/s41598-017-14463-0.
(41) Khorashadizade, E.; Mohajernia, S.; Hejazi, S.; Mehdipour, H.; Naseri, N.; Moradlou, O.; Moshfegh, A. Z.; Schmuki, P. Intrinsically Ru-Doped Suboxide TiO_2 Nanotubes for Enhanced Photoelectrocatalytic H_2 Generation. *J. Phys. Chem. C* **2021**, *125*, 6116−6127.
(42) Kalantari, K.; Kalbasi, M.; Sohrabi, M.; Royaee, S. J. Synthesis and characterization of N-doped TiO_2 nanoparticles and their application in photocatalytic oxidation of dibenzothiophene under visible light. *Ceram. Int.* **2016**, *42*, 14834−14842.
(43) Boningari, T.; Reddy Inturi, S. N.; Suidan, M.; Smirniotis, P. G. Novel one-step synthesis of nitrogen-doped TiO_2 by flame aerosol technique for visible-light photocatalysis: Effect of synthesis parameters and secondary nitrogen (N) source. *Chem. Eng. J.* **2018**, *350*, 324−334.
(44) Asahi, R.; Morikawa, T. Nitrogen complex species and its chemical nature in TiO_2 for visible-light sensitized photocatalysis. *Chem. Phys.* **2007**, *339*, 57−63.
(45) Di Valentin, C.; Finazzi, E.; Pacchioni, G.; Selloni, A.; Livraghi, S.; Paganini, M. C.; Giamello, E. N-doped TiO_2: Theory and experiment. *Chem. Phys.* **2007**, *339*, 44−56.
(46) Han, K. S.; Lee, D. K.; Lee, J. W.; Lee, G. I.; Kang, J. K. Nature of N 2p, Ti 3d, O 2p Hybridization of N-Doped TiO_2 Nanotubes and Superior Photovoltaic Performance through Selective Atomic N Doping. *Chem. − Eur. J.* **2011**, *17*, 2579−2582.
(47) Asahi, R.; Morikawa, T.; Irie, H.; Ohwaki, T. Nitrogen-Doped Titanium Dioxide as Visible-Light-Sensitive Photocatalyst: Designs, Developments, and Prospects. *Chem. Rev.* **2014**, *114*, 9824−9852.
(48) Zatsepin, D. A.; Boukhvalov, D. W.; Kurmaev, E. Z.; Zhidkov, I. S.; Gavrilov, N. V.; Korotin, M. A.; Kim, S. S. Structural defects and electronic structure of N-ion implanted TiO_2:Bulk versus thin film. *Appl. Surf. Sci.* **2015**, *355*, 984−988.
(49) Antony, R. P.; Mathews, T.; Ajikumar, P. K.; Krishna, D. N.; Dash, S.; Tyagi, A. K. Electrochemically synthesized visible light absorbing vertically aligned N-doped TiO2 nanotube array films. *Mater. Res. Bull.* **2012**, *47*, 4491−4497.
(50) Hou, X.; Liu, F.; Yao, K.; Ma, H.; Deng, J.; Li, D.; Liao, B. Photoelectrical properties of nitrogen doped TiO2 nanotubes by anodic oxidation of N^+ implanted Ti foils. *Mater. Lett.* **2014**, *124*, 101−104.
(51) Mohan, L.; Anandan, C.; Rajendran, N. Effect of plasma nitriding on structure and biocompatibility of self-organised TiO_2 nanotubes on Ti−6Al−7Nb. *RSC Adv.* **2015**, *5*, 41763−41771.
(52) Hanzu, I.; Djenizian, T.; Knauth, P. Electrical and Point Defect Properties of TiO_2 Nanotubes Fabricated by Electrochemical Anodization. *J. Phys. Chem. C* **2011**, *115*, 5989−5996.
(53) Matsuda, S.; Kato, A. Titanium oxide based catalysts - a review. *Appl. Catal.* **1983**, *8*, 149−165.
(54) Kruse, N.; Chenakin, S. XPS characterization of Au/TiO_2 catalysts: Binding energy assessment and irradiation effects. *Appl. Catal., A* **2011**, *391*, 367−376.
(55) Hejazi, S.; Nguyen, N. T.; Mazare, A.; Schmuki, P. Aminated TiO_2 nanotubes as a photoelectrochemical water splitting photoanode. *Catal. Today* **2017**, *281*, 189−197.
(56) Liu, G.; Jaegermann, W.; He, J.; Sundstrom, V.; Sun, L. XPS and UPS Characterization of the TiO_2/ZnPcGly Heterointerface: Alignment of Energy Levels. *J. Phys. Chem. B* **2002**, *106*, 5814−5819.
(57) Wu, Z.; Dong, F.; Zhao, W.; Wang, H.; Liu, Y.; Guan, B. The fabrication and characterization of novel carbon-doped TiO_2 nanotubes, nanowires and nanorods with high visible light photocatalytic activity. *Nanotechnology* 2009, *20*, 235701(9 pages), DOI: 10.1088/0957-4484/20/23/235701.
(58) Humbert, P.; Deville, J. P. Oxygen Auger spectra of some transition-metal oxides: relaxation energies and d-band screening. *J. Phys. C: Solid State Phys.* **1987**, *20*, 4679−4687.
(59) Rumaiz, A. K.; Woicik, J. C.; Cockayne, E.; Lin, H. Y.; Jaffari, G. H.; Shah, S. I. Oxygen vacancies in N doped anatase: Experiment and

first-principles calculations. *Appl. Phys. Lett.* **2009**, *95*, 262111-1−262111-3.
(60) Fusi, M.; Maccallini, E.; Caruso, T.; Casari, C. S.; Bassi, A. L.; Bottani, C. E.; Rudolf, P.; Prince, K. C.; Agostino, R. G. Surface electronic and structural properties of nanostructured titanium oxide grown by pulsed laser deposition. *Surf. Sci.* **2011**, *605*, 333−340.
(61) Pan, X.; Yang, M.-Q.; Fu, X.; Zhang, N.; Xu, Y.-J. Defective TiO_2 with oxygen vacancies: synthesis, properties and photocatalytic applications. *Nanoscale* **2013**, *5*, 3601−3614.
(62) Zawadzki, P. Absorption Spectra of Trapped Holes in Anatase TiO_2. *J. Phys. Chem. C* **2013**, *117*, 8647−8651.
(63) Schneider, J.; Matsuoka, M.; Takeuchi, M.; Zhang, J.; Horiuchi, Y.; Anpo, M.; Bahnemann, D. W. Understanding TiO_2 Photocatalysis: Mechanisms and Materials. *Chem. Rev.* **2014**, *114*, 9919−9986.
(64) Powell, C. J.; Jablonski, A. *NIST Electron Inelastic-Mean-Free-Path Database SRD 71, Ver. 1.2*; NIST: Gaithersburg, MD, 2010, https://www.nist.gov/srd/nist-standard-reference-database-71.
(65) Ozkan, S.; Mazare, A.; Schmuki, P. Extracting the limiting factors in photocurrent measurements on TiO_2 nanotubes and enhancing the photoelectrochemical properties by Nb doping. *Electrochim. Acta* **2015**, *176*, 819−826.
(66) Lee, K.; Schmuki, P. Bottom sealing and photoelectrochemical properties of different types of anodic TiO_2 nanotubes. *Electrochim. Acta* **2013**, *100*, 229−235.
(67) Jiang, X.; Wang, Y.; Pan, C. High Concentration Substitutional N-Doped TiO_2 Film: Preparation, Characterization, and Photocatalytic Property. *J. Am. Ceram. Soc.* **2011**, *94*, 4078−4083.
(68) Seiß, V.; Helbig, U.; Lösel, R.; Eichelbaum, M. Investigating and correlating photoelectrochemical, photocatalytic, and antimicrobial properties of TiO_2 nanolayers. *Sci. Rep.* 2021, *11*, 22200(16 pages), DOI: 10.1038/s41598-021-01165-x.
(69) Beranek, R.; Tsuchiya, H.; Sugishima, T.; Macak, J. M.; Taveira, L.; Fujimoto, S.; Kisch, H.; Schmuki, P. Enhancement and limits of the photoelectrochemical response from anodic TiO_2 nanotubes. *Appl. Phys. Lett.* **2005**, *87*, 243114-1−243114-3.

https://doi.org/10.1021/acsanm.3c01278
ACS Appl. Nano Mater. 2023, 6, 10351−10364